PNAS RESEARCH ARTICLE | CELL BIOLOGY

Mec1 regulates PAS recruitment of Atg13 via direct binding with Atg13 during glucose starvation-induced autophagy

Weijing Yao[a,1], Yixing Li[a,1], Yingcong Chen[a,1], Yuting Chen[a,1], Pengwei Zhao[a], Yi Zhang[a], Qiang Jiang[a], Yuyao Feng[a], Fan Yang[a], Choufei Wu[b], Huiming Zhong[c], Yiting Zhou[a], Qiming Sun[a], Liqin Zhang[b], Wei Liu[a], and Cong Yi[a,2]

Edited by James Haber, Brandeis University, Waltham, MA; received September 7, 2022; accepted November 15, 2022

Mec1 is a DNA damage sensor, which performs an essential role in the DNA damage response pathway and glucose starvation-induced autophagy. However, the functions of Mec1 in autophagy remain unclear. In response to glucose starvation, Mec1 forms puncta, which are recruited to mitochondria through the adaptor protein Ggc1. Here, we show that Mec1 puncta also contact the phagophore assembly site (PAS) via direct binding with Atg13. Functional analysis of the Atg13–Mec1 interaction revealed two previously unrecognized protein regions, the Mec1-Binding Region (MBR) on Atg13 and the Atg13-Binding Region (ABR) on Mec1, which mediate their mutual association under glucose starvation conditions. Disruption of the MBR or ABR impairs the recruitment of Mec1 puncta and Atg13 to the PAS, consequently blocking glucose starvation-induced autophagy. Additionally, the MBR and ABR regions are also crucial for DNA damage-induced autophagy. We thus propose that Mec1 regulates glucose starvation-induced autophagy by controlling Atg13 recruitment to the PAS.

Mec1 | Atg13 | glucose starvation-induced autophagy | *Saccharomyces cerevisiae*

Autophagy is a highly conserved vacuole- or lysosome-dependent catabolic process. It is primarily focused upon the destruction of damaged, or redundant cellular components including aggregates, exogenous pathogens, lipid droplets, or damaged organelles such as mitochondria, ribosomes, or endoplasmic reticulum (1). It has an essential role in maintaining cell homeostasis and organismal growth and development, and autophagic dysfunction has been closely linked to many human diseases, including neurodegenerative diseases, obesity, and tumorigenesis (2). The process of autophagy is coordinated in a stepwise fashion, which each step requiring the coordination of specific proteins and complexes. In particular, the Atg1 complex participates in the assembly of the phagophore assembly site (PAS) and the initiation of autophagy, the PI3K complex I (Vps34-Vps15-Atg6-Atg14) is responsible for phosphatidylinositol 3-phosphate (P13P) production and the recruitment of the effector protein Atg18, while Atg9 vesicles in providing the membrane source for autophagosomal biogenesis (1).

The maintenance of glucose homeostasis has recently been emerging as one of the most important physiological roles for autophagy (3). The question of how autophagy senses and responds to glucose starvation is therefore central to the understanding of its molecular mechanisms and roles in related diseases. While great progress has been made in the study of autophagy induced by nitrogen or amino acid starvation, far less is known about the molecular mechanisms and functions of glucose starvation-induced autophagy (4–7). Recently, our group found that Mec1 is necessary for autophagy specifically induced by glucose starvation (8). Mec1, a member of the Phosphoinositides (PI) kinase superfamily, is essential for sensing DNA damage signals and initiating the DNA damage repair signaling pathway (9). In response to glucose starvation, an increase in reactive oxygen species (ROS) physiologically induces the formation of Mec1 puncta (10). Subsequently, Mec1 puncta are recruited to the mitochondria through the adaptor protein Ggc1. Snf1, a yeast homolog of the intracellular energy sensor Adenosine 5'-monophosphate (AMP)-activated protein kinase (AMPK) then phosphorylates Mec1 on the mitochondria surface to maintain aerobic respiration, which is crucial for enhancing the association of Atg1 with Atg13 to initiate glucose starvation-induced autophagy (8). Nevertheless, a fuller understanding of the roles and molecular mechanisms of Mec1 in glucose starvation-induced autophagy awaits further investigation.

Atg13, an essential protein of the core autophagic machinery, is highly phosphorylated by mTORC1 in nutrient-rich media. However, under starvation or rapamycin treatment conditions, Atg13 is rapidly dephosphorylated, which then leads to enhanced Atg1–Atg13 interaction, as well as Atg13–Atg17 binding, culminating in the formation of the Atg1 kinase complex. Once activated, the Atg1 kinase complex will then recruit other downstream Atg proteins to initiate autophagosome formation (1). In addition to mTORC1, cyclic adenosine 5'-monophosphate (cAMP)-dependent protein kinase can also

Significance

Maintaining glucose homeostasis is one of the most important physiological functions of autophagy. However, little is known about the molecular mechanism of glucose starvation-induced autophagy. In this study, we found that Mec1, a DNA damage sensor, forms puncta to contact with the PAS under glucose starvation. Further studies found that Mec1 participates in glucose starvation-induced autophagy through direct interaction with Atg13, the Mec1-Binding Region (MBR). The absence of this region blocks the PAS recruitment of Mec1 puncta and Atg13. Intriguingly, we found that Mec1–Atg13 binding is also required for DNA damage-induced autophagy via mediating the PAS recruitment of Atg13. These results indicate that Mec1–Atg13 direct binding is a crucial step in glucose starvation-induced autophagy.

Author contributions: W.Y., Y.L., and C.Y. designed research; W.Y., Y.L., Y.C.C., Y.T.C., P.Z., Y.Zhang., Q.J., Y.F., and F.Y. performed research; F.Y. and Y.Zhou. contributed new reagents/analytic tools; W.Y., Y.L., Y.C.C., Y.T.C., P.Z., Y. Zhang, C.W., H.Z., Y. Zhou, Q.S., L.Z., W.L., and C.Y. analyzed data; and C.Y. wrote the paper.

The authors declare no competing interest.

This article is a PNAS Direct Submission.

[1]W.Y., Y.L., Yingcong Chen, and Yuting Chen contributed equally to this work.

[2]To whom correspondence may be addressed. Email: yiconglab@zju.edu.cn.

This article contains supporting information online at https://www.pnas.org/lookup/suppl/doi:10.1073/pnas.2215126120/-/DCSupplemental.

Published December 27, 2022.

phosphorylate Atg13 to block the initiation of autophagy (11, 12). Recently, Protein phosphatase 2C (PP2C)-type phosphatases were shown to act in Atg1 and Atg13 dephosphorylation. Deletion of the PP2C-type phosphatase genes *PTC2* and *PTC3* resulted in impairment of autophagic activity via the accumulation of hyperphosphorylated Atg1 and Atg13 (13). Atg13 has also been reported to act as a scaffold protein required for the regulation of autophagy. During autophagosome formation, the Atg13 HORMA domain mediates the recruitment of Atg9 vesicles and PI3K complex I to the PAS (14, 15), while Atg1, Atg17, and Vac8 bind directly to differing regions of the Atg13 protein carboxy terminus. All mutations or deletions that have been reported to abolish the binding of these proteins with Atg13 result in severe impairment of autophagic activity, strongly suggesting these regions of Atg13 as major contributors to the initiation of autophagy (16–18). However, it remains unclear whether, and if so to what extent, other proteins can bind directly with Atg13 to regulate autophagy.

In this study, we show that Mec1 regulates glucose starvation-induced autophagy through binding directly to Atg13. By revealing a strong link between the Mec1–Atg13 interaction region and the PAS recruitment of Mec1 puncta and Atg13, we propose that Mec1 serves as a partner for Atg13 to link mitochondria and autophagosomes in the regulation of autophagy under glucose starvation conditions.

Results

Mec1 Directly Binds with Atg13. In the light of previous studies showing an association between Mec1 and Atg1/Atg13, we were led to explore whether Mec1 puncta colocalize with autophagosomes (8). Since Atg17 is a widely used marker protein of the PAS (14), we examined the spatial relationship between Mec1 puncta and Atg1, Atg13, or Atg17 under conditions of nutrient rich or glucose starvation. As shown in Fig. 1 *A*–*C* and *SI Appendix*, Fig. S1, glucose deprivation triggers Mec1 puncta to contact Atg17, Atg1, and Atg13, with colocalization spots as indicated by the yellow signal. About 25% of cells showed this close contact according to the statistical analysis of 3D imaging data (Fig. 1 *D*–*F*), indicating that Mec1 puncta was recruited to the PAS upon glucose starvation. Since Mec1 puncta have also been shown to be recruited to mitochondria at an early stage of glucose starvation (8), we sought to determine whether Mec1 puncta contacts both mitochondria and the PAS under glucose starvation, and if so, consider if this contact is specific to glucose starvation. Using 3D fluorescence imaging and statistical quantification, we confirmed that this was indeed the case (Fig. 1*G* and *SI Appendix*, Figs. S2 and S3 *A* and *B*). Biochemical analysis further confirmed that Atg13 and Atg17 protein localization on mitochondria significantly increased under glucose starvation conditions (*SI Appendix*, Fig. S3*C*), which was consistent with our previous report that showed similar increases on the mitochondrial localization of Atg1, Atg13, and Mec1 levels upon glucose starvation (8). We then tested whether Mec1 mediates linkage between the PAS and mitochondria in response to glucose starvation. As shown in Fig. 1*H* and *SI Appendix*, Fig. S3*D*, the degradation of Mec1 by indole-3-acetic acid (IAA) led to a significant increase in the distance between mitochondria and the PAS under glucose starvation. Furthermore, upon the purification of mitochondria in auxin-inducible degradation (AID)-Mec1 cells coexpressing Om45-Cherry, Atg17-2×Green fluorescent protein (GFP), and HA-Atg13, western blot results showed that under glucose starvation, the amounts of Atg13 and Atg17 on the mitochondria of AID-Mec1 cells treated with IAA were significantly lower as compared with those of cells without IAA treatment (*SI Appendix*, Fig. S3*E*), suggesting that Mec1 is required for mitochondria to link with the PAS under glucose starvation.

To investigate which protein mediates recruitment of Mec1 to the PAS, we performed immunoprecipitation assays to better understand the spatial relationship between Atg1–Atg13 and Mec1. To this end, we co-expressed 3×FLAG-Mec1 and Atg13-2×HA in wild-type (WT) or *atg1*Δ yeast cells, then pulled down Atg13-2×HA using anti-HA agarose beads and used western blot to examine whether 3×FLAG-Mec1 protein could coprecipitate with Atg13 in the absence of *ATG1*. As shown in Fig. 1*I*, no significant difference was found in the ability of Mec1 to bind with Atg13 in *atg1*Δ yeast cells compared with WT cells under either nutrient-rich or glucose starvation conditions. These results indicated that the association of Mec1 with Atg13 was independent of Atg1. Using the same approach, Atg1-3×FLAG and 3×HA-Mec1 were coexpressed in both WT and *atg13*Δ yeast cells. We noted that under nutrient-rich conditions, the binding of Atg1 with Mec1 in the *atg13*Δ background had increased dramatically compared with that in WT cells (*SI Appendix*, Fig. S4*A*), which suggested that Atg13 negatively regulates Mec1 binding to Atg1. These results prompted us to test whether the adaptor protein, Atg11, was involved in this interaction under nutrient-rich conditions. Co-IP assays showed that the association between Mec1 and Atg1 was significantly decreased under the nutrient-rich medium (*SI Appendix*, Fig. S4*B*), indicating that Atg11 positively regulates Mec1-Atg1 binding under nutrient-rich conditions. Yeast two-hybrid (Y2H) assays were then used to screen for Atg1 complex proteins that may directly interact with Mec1, the result showed that only the AH109 strain coexpressing Mec1-AD with Atg13-BD could grow on agar plates containing 3-AT (Fig. 1*J* and *SI Appendix*, Fig. S4*C*), thus leading us to conclude that Mec1 could directly bind with Atg13.

We then investigated the molecular mechanisms driving the increased binding of Mec1-Atg13 under glucose starvation conditions. In previous work, we had found that Snf1-mediated Mec1 phosphorylation to be required for Mec1–Atg1 binding, but not for the interaction between Mec1 and Atg13 in response to glucose starvation (8). Given that ROS and mitochondrial Ggc1 are required for the formation of Mec1 puncta and for the recruitment of Mec1 puncta to mitochondria, respectively, we next tested whether the increased Mec1–Atg13 binding requires ROS or Ggc1. Co-IP assays showed that either treatment with the ROS scavenger, BHA, or the deletion of *GGC1*, completely blocked the glucose starvation-induced increases in Mec1–Atg13 binding (*SI Appendix*, Fig. S4 *D* and *E*). Since Atg11 is crucial for Atg1 complex formation under glucose starvation (19), we then knocked out *ATG11* or generated *ATG1ATG11* double knockouts in WT cells coexpressing 3×FLAG-Mec1 and 2×HA-Atg13. Co-IP results showed *atg11*Δ with significantly lesser increases in Mec1–Atg13 association under glucose starvation conditions, while significant increase in Mec1-Atg13 association was completely inhibited in *atg11*Δ *atg1*Δ cells (*SI Appendix*, Fig. S4*F*). Taken together, these data suggested that the formation of Mec1 puncta, the mitochondrial recruitment of Mec1 puncta, and Atg11 are three key factors required for the increased binding of Mec1–Atg13 in response to glucose starvation.

The Atg13 461-474 aa and Mec1 141-160aa Regions Are Responsible for the Interaction of Mec1–Atg13. Previous structural analysis of Atg13 showed that this protein consists of two structural regions: an N-terminal HORMA domain and a C-terminal disordered region (15). To explore which of these regions were required for its binding with Mec1, we generated two truncation mutants, each carrying one of these domains, for

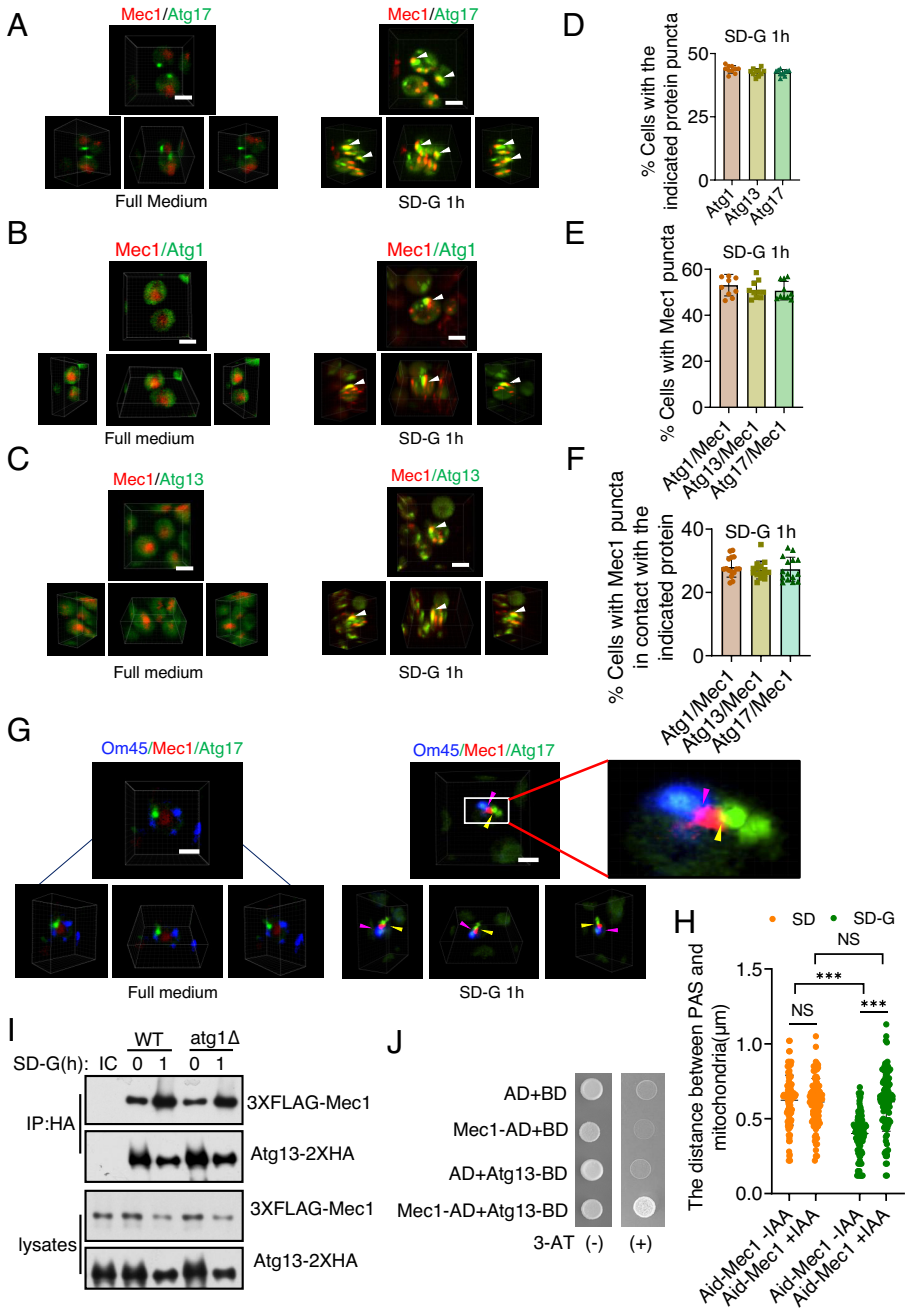

Fig. 1. Mec1 directly binds with Atg13. (*A*–*C*) Cells coexpressing mCherry-Mec1 and (*A*) Atg17-2×GFP, (*B*) Atg1-2×GFP, or (*C*) Atg13-2×GFP were subjected to glucose starvation for 0 h (*Left*) and 1 h (*Right*). 3D imaging produced with spinning disk confocal microscopy was used to observe the spatial localizations. (Scale bar, 5 μm.) (*D*) The number of cells with Atg1, Atg13, or Atg17 puncta under glucose starvation (SD-G) in (*A*–*C*) was quantified. n = 300 cells pooled from three independent experiments. Data are presented as mean ± SD. (*E*) The number of cells in the SD-G treatment with mCherry-Mec1 puncta in (*A*–*C*) was quantified. n = 300 cells pooled from three independent experiments. Data are presented as mean ± SD. (*F*) The number of cells in the SD-G treatment with Mec1 puncta in contact with Atg1, Atg13, or Atg17 in (*A*–*C*) was quantified. n = 300 cells coexpressing mCherry-Mec1 puncta and Atg1, Atg13, or Atg17-2×GFP pooled from three independent experiments. Data are presented as mean ± SD. (*G*) Yeast cells coexpressing Om45-BFP (mitochondrial marker), mCherry-Mec1, and Atg17-2×GFP (PAS marker) were grown to early log phase and then subjected to glucose starvation for 0 h and 1 h. 3D imaging produced with spinning disk confocal microscopy was used to observe their spatial localization. (Scale bar, 5 μm.) (*H*) Cells from *SI Appendix*, Fig. S3*D* were quantified for their respective distances between mitochondria and the PAS. The distance between mitochondria and the PAS was quantified by calculating the distance from the center of Atg17-2×GFP puncta to the centre of the mitochondrial nearest to it, using Image J software. n = 100 cells coexpressing Om45-mCherry and Atg17-2×GFP pooled from three independent experiments. Data are presented as mean ± SD. ***$P < 0.001$, NS, no significance. Two-tailed Student's *t* tests were used. (*I*) WT or *atg1*Δ yeast cells coexpressing 3×FLAG-Mec1 and Atg13-2×HA were starved with SD-G for 0 h and 1 h. Cell lysates were immunoprecipitated using anti-HA agarose beads and then analyzed using western blot with anti-FLAG antibody. IC: isotype control. (*J*) AH109 strain were transformed with Mec1-AD and Atg13-BD and then grown on SD-Leu-Trp or SD-His-Leu-Trp (3-AT) agar plates at 30 °C for 3 d.

analysis via Y2H assay. Results showed that it was the C-terminal disordered region of Atg13 that was necessary for the Atg13-Mec1 association (Fig. 2*A*).

To better understand the function of the Atg13 C-terminal disordered region in the binding of Atg13 with Mec1 (20) (Fig. 2*B*), we constructed a series of deletion variants for this region and used Y2H assays to determine whether they interacted with Mec1. We found that the Atg13 region between residues 461 and 474 was responsible for Mec1–Atg13 binding (*SI Appendix*, Fig. S5 *A* and *B* and Fig. 2 *C* and *D*). To determine which specific residues

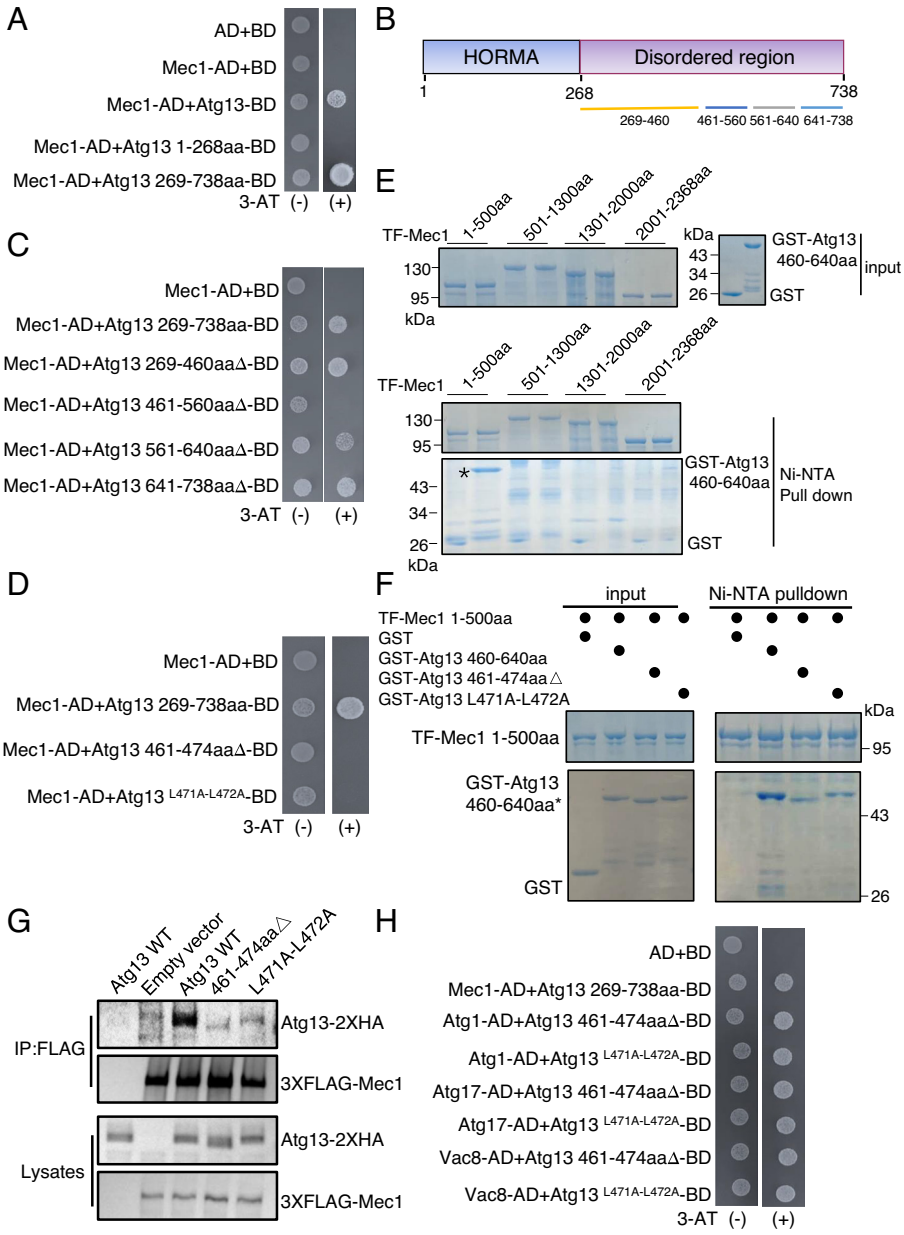

Fig. 2. The Atg13 461-474 aa and Mec1 141-160aa regions are responsible for the binding of Mec1-Atg13. (*A*) The AH109 strain was transformed with plasmids expressing Mec1-AD and plasmids expressing Atg13-BD, Atg13 1–268aa or 269–738aa-BD. These strains were grown on SD-Leu-Trp or SD-His-Leu-Trp (3-AT) agar plates at 30 °C for 3 d. (*B*) The scheme of the Atg13 domains and deletions. (*C* and *D*) The AH109 strain was transformed with plasmids expressing Mec1-AD and plasmids expressing a BD-fused with the indicated deletions or mutations. These strains were grown on SD-Leu-Trp or SD-His-Leu-Trp (3-AT) agar plates at 30 °C for 3 d. (*E*) Ni-nickel-nitrilotriacetic acid (Ni-NTA) pull down of recombinant TF-Mec1 1–500aa, 501–1300aa, 1301–2000aa, or 2001–2368aa with GST or GST–Atg13 460–640aa proteins purified from *E. Coli*. (*F*) Ni-NTA pull down of recombinant TF-Mec1 1–500aa with GST, GST-Atg13 460–640aa WT, 461–474aaΔ, or L471A–L472A proteins purified from *E. Coli*. (*G*) Coexpressing 3×FLAG-Mec1 and empty vector, Atg13-2×HA WT, 461–474aaΔ, or L471A–L472A in *atg13*Δ yeast strains were subjected to glucose starvation for 0 h and 1 h. Cell lysates were immunoprecipitated with anti-FLAG agarose beads and then analyzed by western blot using an anti-HA antibody. (*H*) The AH109 strain was transformed with plasmids expressing Mec1-AD, Atg1-AD, Atg17-AD, or Vac8-AD and plasmids expressing Atg13 269–738aa-BD, 461–474aaΔ-BD, or L471A–L72A-BD. These strains were grown on SD-Leu-Trp or SD-His-Leu-Trp (3-AT) agar plates at 30 °C for 3 d.

mediated the interaction, we then generated random point mutations in this 461–474 aa region to abolish binding with Mec1, the Y2H assays revealed that residues L471 and L472 of Atg13 were crucial for direct Mec1–Atg13 interaction (Fig. 2*D* and *SI Appendix*, Fig. S5 *C* and *D*). To further confirm the 461–474aa region of Atg13 is responsible for Mec1–Atg13 binding, Y2H and in vitro Ni-NTA pulldown assays were performed. Results showed that Mec1 1–500aa could directly bind with Atg13 460–640aa, while binding to the Atg13 460–640aa (461-474aaΔ) or (L471A-L472A) variants was almost undetectable (Fig. 2 *E* and *F* and *SI Appendix*, Fig. S6*A*). Immunoprecipitation experiments further illustrated that the 461–474aa or the L471–L472 region in Atg13 was responsible for Mec1–Atg13 interaction (Fig. 2*G*). We next examined whether disruption of this 461–474 aa region also affected Atg13 binding to Atg1, Atg17, or Vac8, since the Atg13 C-terminal disordered region contains the binding sites for these three (16–18). We then cotransformed a plasmid harboring either the Atg13 461-474aaΔ or L471A-L472A-AD variants with a plasmid carrying either Atg1, Atg13, or Vac8-BD into the AH109 strain and found that the bindings of Atg13 with Atg1, Atg17, and Vac8 were not impaired by the 461-474aaΔ or L471A-L472A mutations (Fig. 2*H*). Taken together, these data confirmed the

461–474aa region of Atg13 as responsible for the binding of Atg13 with Mec1.

Next, to delineate which regions of Mec1 1–500aa are responsible for its binding with Atg13, we constructed a series of deletion mutants in the Mec1 1–1300aa-3×FLAG vector construct. Co-IP assays showed that Mec1 141–160aa is required for Mec1–Atg13 binding during glucose starvation (*SI Appendix*, Fig. S6 *B* and *C*). Subsequently, we used the TF-Mec1 1–500aa or 1–500aa(141-160aaΔ) protein variants purified from *Escherichia coli* for Ni-NTA pulldown assays with GST-Atg13 460–640aa. Results showed that Mec1 1–500aa(141-160aaΔ) displayed dramatically less binding with Atg13 461–640aa than Mec1 1–500aa (*SI Appendix*, Fig. S6*D*). Y2H assays further confirmed that the Mec1 141–160aa region was crucial for Mec1–Atg13 binding (*SI Appendix*, Fig. S6*E*). We next tested the association of Mec1 with Atg13 in yeast cells under the 3×FLAG-Mec1 141–160aaΔ mutant background. Consistent with Y2H and Ni-NTA pulldown results, co-IP experiments highlighted that the FLAG-Mec1 141–160aa region is crucial for Mec1–Atg13 association (*SI Appendix*, Fig. S6*F*). Concurrently, docking simulations of the Mec1-Binding Region (MBR)–Atg13-Binding Region (ABR) by AlphaFold2 indicated that the Atg13 461–474aa region could readily interact with the 141–160aa region of Mec1(*SI Appendix*, Fig. S7). These cumulative results thus provided strong evidence that Atg13 461–474aa and Mec1 141-160aa are the regions responsible for Mec1–Atg13 binding.

Mec1–Atg13 Binding Is Required for Glucose Starvation-Induced Autophagy. Based on the above results, we designated the 461–474aa region of Atg13 as the MBR, and the 141–160aa region of Mec1 as the ABR. To address the role of the Atg13 MBR and Mec1 ABR in autophagy, we first examined the autophagic activity of the Atg13 461–474aaΔ and L471A–L472A variants via GFP-Atg8 localization and cleavage assays. Empty vector, WT Atg13 (WT), or Atg13 variants harboring either 461–474aaΔ or Atg13 L471A–L472A mutations were separately transformed into *atg13*Δ yeast strains coexpressing GFP-Atg8 and Vph1-mCherry. As shown in Fig. 3 *A* and *B*, compared with WT, the number of cells with vacuolar localization of GFP-Atg8 was moderately decreased when coexpressed with either Atg13 461–474aaΔ or L471A–L472A mutants under nitrogen starvation, whereas GFP-Atg8 showed almost no vacuolar localization in

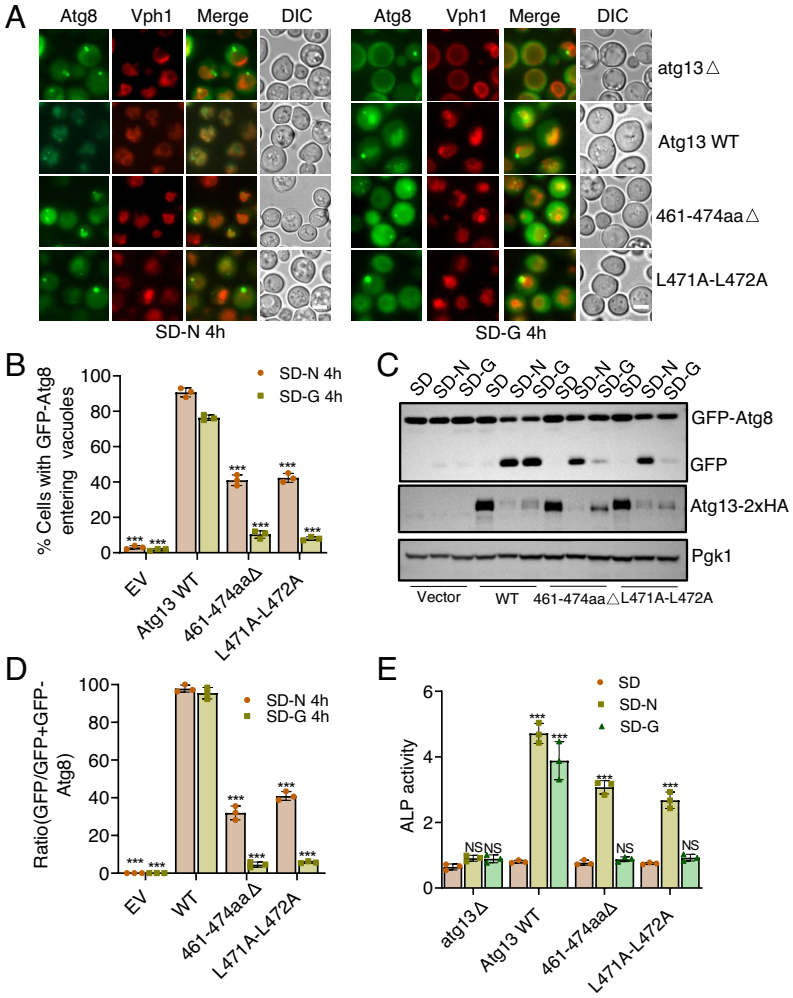

Fig. 3. Mec1-Atg13 binding is necessary for glucose starvation-induced autophagy. (*A*) Empty vector, WT Atg13 (WT), 461–474aaΔ, or L471A–L72A was separately transformed into *atg13*Δ cells expressing GFP-Atg8 and Vph1-Cherry. Cells were subjected to nitrogen starvation (SD-N) or glucose starvation (SD-G) for 4 h, then analyzed using fluorescence microscopy. (Scale bar, 2 μm.) (*B*) Autophagic activity was assessed for the translocation of GFP-Atg8 into vacuoles from (*A*). n = 300 cells pooled from three independent experiments. Data are presented as mean ± SD. ***$P < 0.001$; two-tailed Student's *t* tests were used. (*C*) Autophagic activity from (*A*) was assessed with western blot analysis of the cleavage of GFP-Atg8. Pgk1 served as a loading control. (*D*) The ratio of GFP/GFP+GFP-Atg8 from figure (*C*) was quantified and presented as mean ± SD of three independent experiments. ***$P < 0.001$; two-tailed Student's *t* tests were used. (*E*) In *atg13*Δ, Atg13 WT, 461–474aaΔ, or L471A–L72A cells, ALP activity was tested at 4 h under nitrogen starvation or glucose starvation conditions from n = 3 independent experiments. Error bars indicate SD. ***$P < 0.001$; NS, not significant. Two-tailed Student's *t* tests were used.

these mutants under glucose starvation. Consistent with the imaging data, the expression of either Atg13 mutant resulted in an the almost complete loss of free GFP production under glucose starvation, while free GFP production decreased under nitrogen starvation in these cells compared with that in WT (Fig. 3 *C* and *D*). Concurrently, alkaline phosphatase (ALP) assays were also used to measure autophagic activity. To this end, we separately transformed empty vector, WT Atg13, or Atg13 461–474aaΔ, or L471A-L472A variants into *atg13*Δ ALP yeast strains and found that autophagic activity was dramatically increased in the WT, whereas autophagic activity could not be rescued by either Atg13 variant under glucose starvation conditions (Fig. 3*E*), which was consistent with the results of GFP-Atg8 localization and cleavage assays. Similarly, the Mec1 141–160aa (ABR) contributed to nitrogen starvation-induced autophagy, and is essential for glucose starvation-induced autophagy (*SI Appendix*, Fig. S8 *A–D*). Additionally, we found that Mec1 141–160aaΔ failed to impair its kinase activity in response to methyl methanesulfonate (MMS) treatment (*SI Appendix*, Fig. S8*E*). Based on these results, we thus concluded that the Atg13–Mec1 interaction is essential for glucose starvation-induced autophagy.

Mec1-Atg13 Binding Is Required for the Recruitment of Mec1 puncta and Atg13 to the PAS under Glucose Starvation. In light of the above results showing PAS recruitment of Mec1 puncta under glucose starvation, we next sought to determine whether this process was dependent on Atg13–Mec1 binding. We therefore separately transformed the empty vector, WT Atg13, or Atg13 461-474aaΔ, or L471A-L472A variants into *atg13*Δ cells coexpressing GFP-Mec1 and the PAS marker Atg17-2×mCherry. Fluorescence microscopy with quantitative image analysis showed that WT Atg13 could restore contact between Mec1 puncta and the PAS in the *atg13*Δ background, whereas their contact was almost undetectable in cells transformed with either the Atg13 461–474aaΔ or L471A-L472A mutants under glucose starvation (Fig. 4 *A* and *B* and *SI Appendix*, Fig. S9*A*). Conversely, the deletion of *ATG1* had no effect on the contact between Mec1 puncta and the PAS during glucose starvation (*SI Appendix*, Fig. S9 *B* and *C*). Consistent with this finding, the deletion of the Mec1 ABR also significantly decreased the recruitment of Mec1 puncta to the PAS (*SI Appendix*, Fig. S10 *A* and *B*).

We next investigated which specific step in the Atg protein recruitment process was required for Mec1–Atg13 binding. Previous work has shown that Atg proteins are recruited to the PAS hierarchically during autophagosome formation (21). First, we examined if the binding of Mec1–Atg13 was required for the recruitment of Atg13 to the PAS by separately transforming *atg13*Δ yeast cells expressing Atg17-2 × mCherry with N-terminal GFP-tagged WT Atg13 or the Atg13 461–474aaΔ or L471A–L472A variants. Results clearly showed that GFP-Atg13 WT colocalized with Atg17-2 × mCherry, while GFP-Atg13 puncta was almost completely absent in cells expressing GFP-tagged Atg13 461–474aaΔ or L471A–L472A variants under glucose starvation conditions (Fig. 4 *C* and *D*). Similarly, Atg13 puncta formation was also blocked in the Mec1 141–160aaΔ variant under glucose starvation conditions (*SI Appendix*, Fig. S10 *C* and *D*). Concurrent to the above, we also examined the association of Atg13 with Atg17 in the Atg13–Mec1-binding mutants. Immunoprecipitation assays showed that Atg13–Atg17 binding did not increase in the Atg13 461–474aaΔ or L471A–L472A variants under glucose starvation (Fig. 4*E*). Taken together, these data indicated that the interaction between Mec1 and Atg13 was responsible for the recruitment of Mec1 puncta and Atg13 to the PAS by mediating Atg13 binding with Atg17 under glucose starvation.

Previous studies have reported that Mec1 is crucial for DNA damage-induced autophagy (22). To examine whether the binding of Mec1–Atg13 was also required for DNA damage-induced autophagy, *atg13*Δ yeast cells coexpressing GFP-Atg8 and Vph1-mCherry were transformed with plasmids encoding either the Atg13 461–474aaΔ or L471A–L472A variants, or WT Atg13, or the empty vector, and then treated with the DNA-damaging agent MMS. Fluorescence imaging data and statistical analysis showed that vacuolar localization of GFP-Atg8 was significantly impaired in cells expressing either Atg13 MBR mutant (*SI Appendix*, Fig. S11 *A* and *B*). Consistent with these observations, the free GFP band was almost completely absent in Atg13 MBR mutants under treatment with MMS (*SI Appendix*, Fig. S11*C*). Similarly, using the Mec1 141–160aaΔ, we found that the Mec1 ABR was also shown as crucial for DNA damage-induced autophagy (*SI Appendix*, Fig. S11 *D* and *E*) and further confirming the binding of Mec1 with Atg13 to be important for DNA damage-induced autophagy. Subsequently, we examined the binding of Atg13–Atg17 in *atg13*Δ yeast cells expressing the Atg13 461–474aaΔ or L471A–L472A mutants. Immunoprecipitation assays showed that the association of Atg13 with Atg17 was almost completely lost under exposure to MMS (*SI Appendix*, Fig. S11*F*). In agreement with this finding, imaging data and statistical analysis also showed that recruitment of Atg13 to the PAS was blocked in the Mec1–Atg13-binding mutants under MMS treatment (*SI Appendix*, Fig. S11 *G* and *H*). Based on these lines of evidence, we thus concluded that Mec1 is crucial for DNA damage-induced autophagy via regulating the association of Atg13 with Atg17.

Given that Mec1 puncta are recruited to mitochondria and that Mec1 is important for DNA damage-induced autophagy, we also examined mitophagy and nucleophagy activity in cells harboring the Atg13 461–474aa Δ or L471A–L472A mutants as compared with those in WT Atg13, or the empty vector in *atg13*Δ yeast cells expressing the mitochondrial protein Om45-GFP or the nuclear protein Nop1-GFP. Western blots showed that Mec1–Atg13 binding was also crucial for mitophagy and nucleophagy (*SI Appendix*, Fig. S12).

Discussion

In this study, we identified Mec1 as a previously unknown direct binding partner of Atg13. By clarifying the link between Mec1 and Atg13, our results here, together with our previous findings, show that Mec1 puncta mediate contact between mitochondria and autophagosomes via Ggc1 and Atg13 to regulate the recruitment of Mec1 puncta and Atg13 to the PAS, thus initiating autophagy in response to glucose starvation (Fig. 4*F*).

Given that Atg13 serves as a scaffold protein that regulates the PAS localization of Atg proteins as well as vacuolar localization of the PAS via direct binding with a suite of autophagy-related proteins, an important question that remains is whether there are proteins that directly interact with Atg13 that have not been yet found to participate in autophagy. Here, we found that a previously unknown Atg13 interaction partner, Mec1, participates in the regulation of glucose starvation-induced autophagy through direct binding with Atg13. In this study, we discovered the mechanism by which Mec1 puncta are recruited to the PAS specifically in response to glucose starvation. We also identified the 461–474aa region on Atg13 and the 141–160aa region on Mec1 as necessary for the binding of Mec1 with Atg13, which we thus named the MBR and ABR (Atg13-Binding Region), respectively. Previous reports have shown that Mec1 plays a central role in DNA damage-induced autophagy. Our study showed that the binding of Mec1–Atg13 is also a crucial step in the PAS recruitment of Atg13 and in the subsequent initiation of DNA

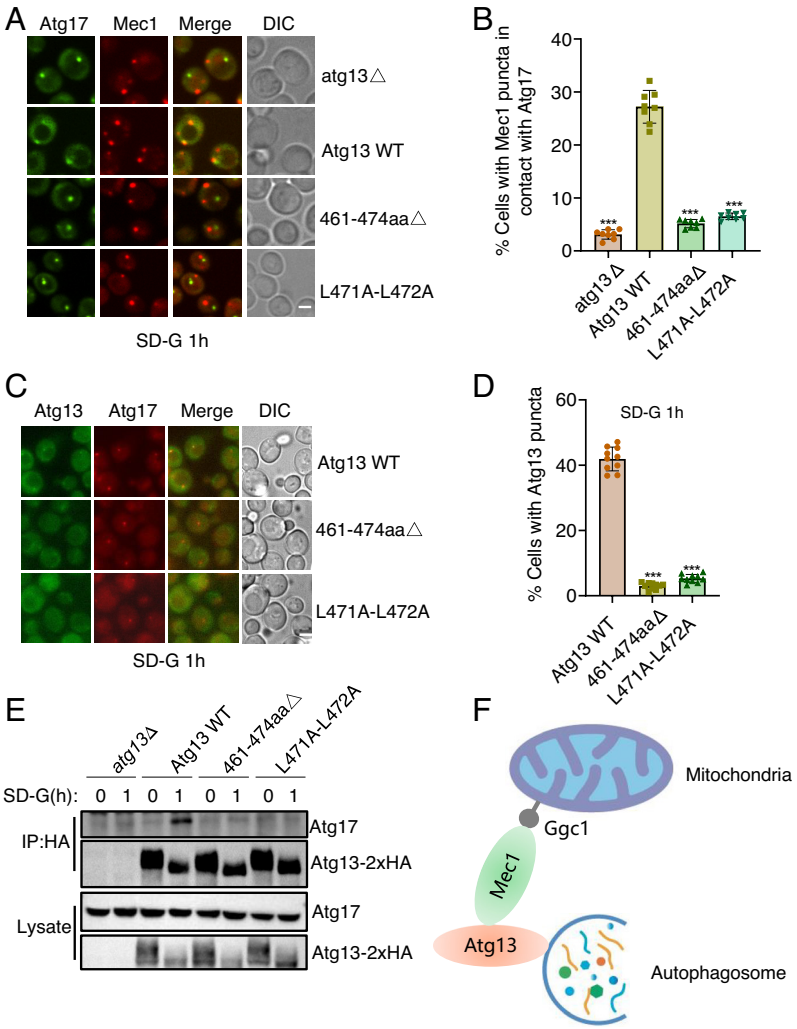

Fig. 4. Mec1-Atg13 binding is responsible for the recruitment of Mec1 puncta and Atg13 to the PAS under glucose starvation. (*A*) empty vector, WT Atg13 (WT), 461–474aaΔ, or L471A–L72A were separately transformed into *atg13*Δ cells coexpressing mCheey-Mec1 and Atg17-2×GFP. Cells were subjected to glucose starvation for 1 h, then analyzed by spinning disk confocal microscopy. (Scale bar, 2 μm.) (*B*) Cells from (*A*) were quantified for the number of cells with mCherry-Mec1 puncta in contact with Atg17-2×GFP. n = 300 cells pooled from three independent experiments. Data are presented as mean ± SD. ***$P < 0.001$; two-tailed Student's *t* tests were used. (*C*) Coexpressing WT Atg13 (WT), 461–474aaΔ, or L471A–L72A with N-terminal GFP-tag and Atg17-2×mCherry in *atg13*Δ cells were grown to log phase and then subjected to glucose starvation for 1 h, then analyzed by microscopy. (Scale bar, 2 μm.) (*D*) Cells from (*C*) were quantified for the number of cells with GFP-Atg13. n = 300 cells pooled from three independent experiments. Data are presented as mean ± SD. ***$P < 0.001$; two-tailed Student's *t* tests were used. (*E*) *atg13*Δ cells expressing empty vector, WT Atg13-2×HA (WT), 461–474aaΔ, or L471A–L72A were subjected to glucose starvation for 0 h and 1 h. Cell lysates were immunoprecipitated with anti-HA agarose beads and then analyzed by western blot using an anti-Atg17 antibody. (*F*) The model map of Mec1 regulating glucose starvation-induced autophagy.

damage-induced autophagy. These results imply that the roles of Mec1 in both glucose starvation- and DNA damage-induced autophagy require its interaction with Atg13 followed by regulation of Atg13 recruitment to the PAS.

Additionally, the Y2H assays showed that the deletion of the Atg13 MBR did not affect Atg13 binding to Atg17, whereas immunoprecipitation experiments indicated that deletion of the Atg13 MBR blocked the increases in binding with Atg17 under glucose starvation conditions. These results thus suggest that the association of Atg13 with Atg17 may be regulated by their post-translational modifications under glucose starvation. We also observed that Atg13 was subjected to proteasomal degradation under starvation conditions. In fact, the absence or hyperactivation of autophagy are harmful to cell survival (23), and autophagic activity has been shown to gradually weaken under prolonged starvation. In yeast, for example, autophagy is weakened to the point of its near absence after 10 to 12 h of nitrogen starvation (24), and proteasomal degradation of Atg13 similarly down-regulates autophagic activity in plant cells treated with long-term starvation (25). This cumulative evidence led us to hypothesize that the degradation of Atg13 by proteasomes can modulate autophagic activity toward the protection of cell survival under prolonged starvation in yeast. It should be noted that the 460–474aa region of Atg13 was previously reported as the Atg13 region responsible for binding with Atg1 (26). However, Y2H and in vitro Ni-NTA pulldown assays in this work indicate that it is the 475–482aa region of Atg13 that in fact mediates its binding with Atg1 (*SI Appendix*, Fig. S13). However, it must be acknowledged that, despite both Y2H and in vitro Ni-NTA pulldown assays supporting the direct binding of Mec1–Atg13, and the fact that Mec1 141–160aaΔ does not impair its kinase activity, we still cannot completely rule out the possibility that this is due to indirect interactions, such as via Ddc2 or other factors that rely on Mec1 integrity or associate with Mec1.

Despite the above results, it remains unknown as to why Mec1 puncta connect mitochondria with autophagosomes to initiate autophagy during glucose starvation. Previous reports have shown

that mitochondria serve as the source of the autophagosome membrane (27), leading us to speculate that mitochondria provide a reservoir of materials with which to form the autophagosomal membrane during glucose starvation. Additionally, in response to glucose starvation, mitochondria serve as production centers for cellular energy, with Snf1/AMPK together to sense changes in cellular energy levels. In order to adapt to this change in the cellular environment, cells must transmit this starvation signal to the downstream effector, which is autophagy, resulting in the recycling of superfluous materials to ensure cell survival. Mec1 thus transmits this signal to the autophagy initiation complex. This mechanism is also consistent with the results of Mec1 phosphorylation by Snf1 on the mitochondrial surface to maintain aerobic respiration under glucose starvation (8).

In summary, we have revealed the role of Mec1 during the process of glucose starvation-induced autophagy. Our results suggest that Mec1 puncta connect mitochondria to autophagosomes through binding with Ggc1 and Atg13 to initiate glucose starvation-induced autophagy. Further studies will be forthcoming to clarify the specific signaling pathway and to determine the source of the autophagosomal membrane occurring in response to glucose starvation.

Materials and Methods

Yeast Strains and Growth Conditions. All yeast strains used in this study are listed in *SI Appendix*, Table S1. Related strains were verified by western blot with corresponding antibody or PCR analysis (Vazyme, P505-d1) (28). All plasmids in this study were sequenced. Yeast cells were cultured at 30 °C in synthetic medium (SD; 0.17% yeast nitrogen base without amino acids and ammonium sulfate, 0.5% ammonium sulfate, 2% glucose, and corresponding auxotrophic amino acids and vitamins). For autophagy induction, cells were cultured to mid-log phase in SD medium and then treated with nitrogen starvation medium (SD-N; 0.17% yeast nitrogen base without amino acids and ammonium sulfate, 2% glucose), glucose starvation medium (SD-G; 0.17% yeast nitrogen base without amino acids and ammonium sulfate, 0.5% ammonium sulfate, 0.5% casamino acid), or 0.04% MMS (Sigma, 129925) for the indicated times at 30 °C.

Antibodies. Antibodies were purchased and used at the indicated dilutions in this study as follows: anti-HA (Abmart, M20003L; 1:3,000), anti-FLAG (Sigma, F1804; 1:2,500), anti-GFP (Roche, 11814460001; 1:2,500), anti-Pgk1 (Nordic Immunology, NE130/7S; 1:10,000), anti-Porin (Invitrogen, 459500, 1:10,000); Anti-Atg17 antibody (gifted from Prof. Yoshinori Ohsumi, Tokyo Institute of Technology, Tokyo); goat anti-mouse IgG1, human ads-HRP (SouthernBiotech, 1070-05; 1:10,000), goat anti-rabbit, human ads-HRP (SouthernBiotech, 4010-05; 1:10,000).

Western Blot, ALP Assay, Immunoprecipitation, and Mitochondrial Purification. Yeast strains were grown to OD_{600} = 0.8–1.2 in nutrient-rich media and treated with nitrogen starvation, glucose starvation, or the DNA damage agent MMS for the indicated times. The extraction of yeast protein, immunoblotting, immunoprecipitation experiments, ALP assays, and mitochondrial purification, were all performed in accordance with previously described methods (8, 29).

Auxin Treatment. Yeast strains with AID tags were treated with 0.5 mm IAA (sigma, I2886) to degrade the targeted protein. An equal amount of dimethyl sulfoxide (DMSO) was added to the corresponding strains as a control (8).

Y2H Assay. A Y2H assay was performed as previously described (30). Briefly, the AH109 strain was transformed with the indicated combinations of pGADT7-originated and pGBKT7-originated plasmids. The related yeast strains were spotted onto SC-leu-Trp and SC-His-Leu-Trp(3-AT) plates with incubation at 30 °C for 2 to 4 d.

In Vitro Ni-NTA Pulldown Assay. TF-Mec1 1-500aa protein or the indicated proteins were incubated with 6 μL Ni-NTA agarose resin in enrichment buffer (50 mM Tris.HCl, pH 7.5, 500 mM NaCl, 0.1% Triton X-100, 0.1 mM PMSF, 1 mM DTT) for 1 h on a rotor at 4 °C. After washing three times, the beads were incubated with GST-Atg13 461–640aa protein, or the other indicated proteins, in a binding buffer (1 mM EDTA, 1 mM EGTA,15 mM $NaH_2P_2O_7$, 0.5% Tween-20, 1× PBS) for 2 h on a rotor at 4 °C. After washing three times, the beads were added to 2× SDS loading buffer. After boiling at 95 °C for 5 min, the samples were separated Sodium Dodecyl Sulphate-Polyacrylamide Gel Electrophoresis (SDS-PAGE) and then stained with Coomassie brilliant blue (31).

Microscopy and Imaging Analysis. Yeast strains with fluorescent tags were grown to OD_{600} = 0.8–1.2 in nutrient-rich media and treated with nitrogen starvation, glucose starvation, or DNA damage agent MMS for the indicated times. Cells were observed using inverted fluorescence microscopy (IX83; Olympus) or spinning disk confocal super resolution microscopy (SpinSR10; Olympus) (8). For 3D imaging, thirty z-stack images at 0.2-μm intervals were taken and deconvolved using the Softworx software. Maximum-intensity projection images of deconvolved data are shown in the corresponding figure. All the images were processed using Fiji ImageJ software and its plugins. ImageJ Scrip was used to calculate the distance between the PAS and mitochondria under full medium, or glucose starvation conditions (32).

Quantitative and Statistical Analysis. ImageJ software was used to quantify the indicated western blot images from three independent experiments (32). Free GFP intensities were quantified by the ratio of band intensities of GFP to those of GFP + GFP-fused protein to calculate the degradation rate of the fused protein (33). All statistical analyses used GraphPad Prism 8 and are presented as mean ± SD (n = 3). For all imaging quantitative analyses, mean values are displayed together with the SD (shown as error bars). The number of independent experiments and cells with coexpressing fluorescent proteins, and the related statistics are indicated in each figure legend. ***$P < 0.001$; **$P < 0.01$; *$P < 0.05$; NS, no significance. Two-tailed Student's *t* tests were used.

Data, Materials, and Software Availability. All study data are included in the article and/or *SI Appendix*.

ACKNOWLEDGMENTS. We are grateful to Prof. Y. Ohsumi, Prof. H. Nakatogawa, and Prof. Zhiping Xie for the plasmids and yeast strains. We thank Prof. Pengfei Xu for providing the spinning disk high-resolution confocal microscope, Prof. Li Yu, Prof. Zhi Hong, Prof. Yixian Cui, and other members of the lab for constructive reading and discussion of the manuscript. The research was supported by National Natural Science Foundation of China (32122028, 92254307, 32070739, 91754107, and 31771528), Zhejiang Provincial Natural Science Foundation of China under Grant No: LR21C070001, and the National Basic Research Program of China (2017YFA0503402) to C.Y., National Natural Science Foundation of China (Grant No: 32100600) to W.Y., and the National Key Research and Development Program of China (2021YFC2600104) to L.Z.

Author affiliations: [a]Department of Biochemistry and Department of Hepatobiliary and Pancreatic Surgery of the First Affiliated Hospital, Zhejiang University School of Medicine, Hangzhou, 310058, China; [b]Key Laboratory of Vector Biology and Pathogen Control of Zhejiang Province, School of Life Sciences, Huzhou University, Huzhou, 313000, China; and [c]Department of Emergency, The Second Affiliated Hospital, Zhejiang University School of Medicine, Zhejiang University, Hangzhou, 310009, China

1. Y. Ohsumi, Historical landmarks of autophagy research. *Cell Res.* **24**, 9–23 (2014).
2. N. Mizushima, B. Levine, Autophagy in human diseases. *N. Engl. J. Med.* **383**, 1564–1576 (2020).
3. G. Karsli-Uzunbas *et al.*, Autophagy is required for glucose homeostasis and lung tumor maintenance. *Cancer Discov.* **4**, 914–927 (2014).
4. T. Fukuda *et al.*, Atg43 tethers isolation membranes to mitochondria to promote starvation-induced mitophagy in fission yeast. *eLife* **9**, e61245 (2020).
5. C. W. Lee *et al.*, Selective autophagy degrades nuclear pore complexes. *Nat. Cell Biol.* **22**, 159–166 (2020).
6. Y. Tomioka *et al.*, TORC1 inactivation stimulates autophagy of nucleoporin and nuclear pore complexes. *J. Cell Biol.* **219**, e201910063 (2020).
7. F. Wilfling *et al.*, A selective autophagy pathway for phase-separated endocytic protein deposits. *Mol. Cell* **80**, 764–778.e767 (2020).
8. C. Yi *et al.*, Formation of a Snf1-Mec1-Atg1 module on mitochondria governs energy deprivation-induced autophagy by regulating mitochondrial respiration. *Dev. Cell* **41**, 59–71.e54 (2017).
9. A. Marechal, L. Zou, DNA damage sensing by the ATM and ATR kinases. *Cold Spring Harb. Perspect. Biol.* **5**, a012716 (2013).

10. C. F. Wu *et al.*, ROS is essential for initiation of energy deprivation-induced autophagy. *J. Genet. Genomics* **48**, 512–515 (2021).
11. Y. Kamada *et al.*, Tor directly controls the Atg1 kinase complex to regulate autophagy. *Mol. Cell. Biol.* **30**, 1049–1058 (2010).
12. J. S. Stephan, Y. Y. Yeh, V. Ramachandran, S. J. Deminoff, P. K. Herman, The Tor and PKA signaling pathways independently target the Atg1/Atg13 protein kinase complex to control autophagy. *Proc. Natl. Acad. Sci. U.S.A.* **106**, 17049–17054 (2009).
13. G. Memisoglu, V. V. Eapen, Y. Yang, D. J. Klionsky, J. E. Haber, PP2C phosphatases promote autophagy by dephosphorylation of the Atg1 complex. *Proc. Natl. Acad. Sci. U.S.A.* **116**, 1613–1620 (2019).
14. S. W. Suzuki *et al.*, Atg13 HORMA domain recruits Atg9 vesicles during autophagosome formation. *Proc. Natl. Acad. Sci. U.S.A.* **112**, 3350–3355 (2015).
15. C. C. Jao, M. J. Ragusa, R. E. Stanley, J. H. Hurley, A HORMA domain in Atg13 mediates PI 3-kinase recruitment in autophagy. *Proc. Natl. Acad. Sci. U.S.A.* **110**, 5486–5491 (2013).
16. D. M. Hollenstein *et al.*, Vac8 spatially confines autophagosome formation at the vacuole in S. cerevisiae. *J. Cell Sci.* **132**, jcs235002 (2019).
17. D. Gatica, X. Wen, H. Cheong, D. J. Klionsky, Vac8 determines phagophore assembly site vacuolar localization during nitrogen starvation-induced autophagy. *Autophagy* **17**, 1636–1648 (2020).
18. Y. Kabeya *et al.*, Atg17 functions in cooperation with Atg1 and Atg13 in yeast autophagy. *Mol. Biol. Cell* **16**, 2544–2553 (2005).
19. W. Yao *et al.*, Atg11 is required for initiation of glucose starvation-induced autophagy. *Autophagy* **16**, 2206–2218 (2020).
20. J. Park *et al.*, Quaternary structures of Vac8 differentially regulate the Cvt and PMN pathways. *Autophagy* **16**, 991–1006 (2020).
21. K. Suzuki, Y. Ohsumi, Current knowledge of the pre-autophagosomal structure (PAS). *FEBS Lett.* **584**, 1280–1286 (2010).
22. V. V. Eapen *et al.*, A pathway of targeted autophagy is induced by DNA damage in budding yeast. *Proc. Natl. Acad. Sci. U.S.A.* **114**, E1158–E1167 (2017).
23. G. Kroemer, B. Levine, Autophagic cell death: The story of a misnomer. *Nat. Rev.* **9**, 1004–1010 (2008).
24. S. Kira *et al.*, Vacuolar protein Tag1 and Atg1-Atg13 regulate autophagy termination during persistent starvation in S. cerevisiae. *J. Cell Sci.* **134**, jcs253682 (2021).
25. H. Qi *et al.*, Arabidopsis SINAT proteins control autophagy by mediating ubiquitylation and degradation of ATG13. *Plant Cell* **32**, 263–284 (2020).
26. Y. Fujioka *et al.*, Structural basis of starvation-induced assembly of the autophagy initiation complex. *Nat. Struct. Mol. Biol.* **21**, 513–521 (2014).
27. D. W. Hailey *et al.*, Mitochondria supply membranes for autophagosome biogenesis during starvation. *Cell* **141**, 656–667 (2010).
28. C. Janke *et al.*, A versatile toolbox for PCR-based tagging of yeast genes: New fluorescent proteins, more markers and promoter substitution cassettes. *Yeast* **21**, 947–962 (2004).
29. C. Yi *et al.*, Function and molecular mechanism of acetylation in autophagy regulation. *Science* **336**, 474–477 (2012).
30. K. Okamoto, N. Kondo-Okamoto, Y. Ohsumi, Mitochondria-anchored receptor Atg32 mediates degradation of mitochondria via selective autophagy. *Dev. Cell* **17**, 87–97 (2009).
31. F. Wilfling *et al.*, A selective autophagy pathway for phase-separated endocytic protein deposits. *Mol. Cell* **80**, 764–778.e767 (2020).
32. J. Schindelin *et al.*, Fiji: An open-source platform for biological-image analysis. *Nat. Methods* **9**, 676–682 (2012).
33. W. Yao *et al.*, Atg1-mediated Atg11 phosphorylation is required for selective autophagy by regulating its association with receptor proteins. *Autophagy* **15**, 1–9 (2022).